Electr Eng
DOI 10.1007/s00202-017-0563-x

ORIGINAL PAPER

Coordinated distribution network control of tap changer transformers, capacitors and PV inverters

Oğuzhan Ceylan[1] · **Guodong Liu**[2] · **Kevin Tomsovic**[3]

Received: 18 January 2017 / Accepted: 16 May 2017

Abstract A power distribution system operates most efficiently with voltage deviations along a feeder kept to a minimum and must ensure all voltages remain within specified limits. Recently with the increased integration of photovoltaics, the variable power output has led to increased voltage fluctuations and violation of operating limits. This paper proposes an optimization model based on a recently developed heuristic search method, grey wolf optimization, to coordinate the various distribution controllers. Several different case studies on IEEE 33 and 69 bus test systems modified by including tap changing transformers, capacitors and photovoltaic solar panels are performed. Simulation results are compared to two other heuristic-based optimization methods: harmony search and differential evolution. The simulation results show the effectiveness of the method and indicate the usage of reactive power outputs of PVs facilitates better voltage magnitude profile.

✉ Oğuzhan Ceylan
oguzhan.ceylan@kemerburgaz.edu.tr

Guodong Liu
gliu@ornl.gov

Kevin Tomsovic
tomsovic@utk.edu

[1] Istanbul Kemerburgaz University, Istanbul, Turkey

[2] Oak Ridge National Laboratory, Oak Ridge, TN, USA

[3] University of Tennessee Knoxville, Knoxville, TN, USA

Keywords Smart grid · Grey wolf optimization · Distributed generation · Voltage regulation

1 Introduction

Power systems are facing dramatic changes. Interest in renewables is rapidly increasing with global new investment in renewable energy of 285.9 billion in 2015, more than 6 times the investment in 2004 [1]. In the past, investment in renewables was seen as expensive and mostly undertaken by developed countries; however, investment from developing countries has been more than the developed countries since 2015 [1]. This can place great economic stress on utilities for a number of reasons, and so it will be critical to take advantage of traditional existing control devices and limiting new infrastructure investment.

Among renewables, solar photovoltaic (PVs) panels are quickly becoming popular. PVs may be classified into three subcategories according to their sizes: utility-scale PVs of 1–10 MW, medium-scale PVs of 10–1000 kW, and small-scaled PVs of up to 10 kW [2]. Traditionally, power distribution systems are designed as radial systems, and the classical "install and forget" philosophy of the power distribution systems must change with high levels of PVs. Among the additional challenges is the significant variations in PV outputs. Accordingly, the operation and control of the distribution system needs to be more active. Classical approach to control voltage deviations in distribution systems is to use tap changer transformers and switched bank capacitors either by timers or open loop controls [3]. Frequent tap changes and switching create additional wear on traditional devices. With recent

Published online: 08 June 2017

technological developments, the lifetime of voltage regulated transformers is increasing [4]. The new technology uses mechanical switch during steady state, and a semiconductor switch during tap change to reduce aging [5]. This brings additional flexibility for optimal operation where such capabilities are available. Another method to control voltage is to use the reactive power supply from PV power electronics-based inverters. As known, currently the participation of rooftop PVs in optimal operation of distribution system is not much since their power factors are generally set to one; however, with new regulations such as California Rule 21 [6] they will be used more and more in a flexible way.

As an extension to our previous works [7,8], this paper optimizes the voltage profile in power distribution systems. Optimization problems may be solved by using the classical methods of differential calculus, iterative numerical techniques or various modern methods of optimization [9]. Generally, iterative numerical optimization methods are based on derivatives. Many modern methods of optimization employ derivative-free techniques. Among the derivative-free methods, population-based methods have gained popularity. These include the well-known genetic algorithm inspired by the evolution process in the nature [10], differential evolution [11], harmony search [12], particle swarm optimization [13] . The population methods generally create an initial solution candidate vectors, and by using operators, such as, crossover, mutation, new and better solution candidate vectors are formed. A recently developed method is inspired by the hunting process of the grey wolves [14], where numerical results of several optimization benchmark functions composed of unimodal, multimodal, fixed dimension multimodal, composite ones and classical engineering optimization problems such as tension/compression spring design, welded beam design, pressure vessel design are compared to other heuristic methods. From the numerical results, this recently developed method performs better than the other heuristics such as particle swarm optimization, genetic algorithms differential evolution in most of the classical methods and is competitive to all of them. The method gives better objective function values for all classical optimization methods. Application of the method to a real-world problem: optical buffer design problem states that the method has the ability to solve real engineering problems. A binary version of the grey wolf optimization algorithm (GWO) is proposed for feature selection problems [15]. A detailed review of derivative-free methods may be found in [16].

In the existing literature, there are several derivative optimization-based methods [17–21] used for optimal operation of power distribution systems. Generally, these approaches are either based on nonlinear programming or on using sensitivity coefficients of the system and solving optimization problem. Applications of population-based methods to distribution systems are too numerous [22] to review here. GWO method has been successfully applied to maximum power point tracking model for PV systems in [23]. Optimal sizing of storage device in a microgrid aiming to minimize operation costs was also performed [24]. Some well-known power systems problems such as economic dispatch problem [25], reactive power dispatch problem [26] were also solved by a GWO algorithm.

In this paper, we

- develop a 15 min interval daily voltage optimization model using GWO;
- evaluate solutions on IEEE 33 and 69 bus test systems simulating several test cases in order to see the effects of voltage control devices, specifically:
  - Case 1: only tap changers of voltage regulators,
  - Case 2: both tap changers of voltage regulators and bank capacitors,
  - Case 3: tap changers of voltage regulators, bank capacitors and inverter-based PVs;
- compare results with a differential evolution [11] and a harmony search [12] method.

2 Optimization model

The objective function aims to minimize voltage deviations from the nominal rating. Voltage regulation is initially performed by using only tap changers of the voltage regulators. Capacitors are included in the voltage regulation process in the next step. Finally, inverter-based PVs are also used to improve the voltage profile.

2.1 Optimization using regulators only

This case considers only tap changers in the voltage regulation process. The mathematical representation of the optimization model is as follows:

$$\begin{aligned} \underset{X}{\text{minimize}} \quad & \sum_{i=1}^{N} ||V_i - 1|| \\ \text{subject to} \quad & 0.95 \leq V_i \leq 1.05 \\ & \mathrm{T}^{\min} \leq \mathrm{T}_i \leq \mathrm{T}^{\max} \end{aligned} \tag{1}$$

where V_i represents the voltage magnitude of bus i, T_i represents the tap position of the regulator, $T^{\min}$ represents the minimum position and $T^{\max}$ represents the maximum position. Note that in Eq. (1), 1 may be easily replaced by nominal voltage.

2.2 Optimization using regulators and capacitors

This case considers both tap changers and capacitors in the voltage regulation process. Mathematical representation of

the optimization model is shown below.

$$\begin{aligned} \underset{X}{\text{minimize}} \ & \sum_{i=1}^{N} ||V_i - 1|| \\ \text{subject to} \ & 0.95 \leq V_i \leq 1.05 \\ & \mathrm{T}^{\min} \leq \mathrm{T}_i \leq \mathrm{T}^{\max} \\ & 0 < \mathrm{C}_i < \mathrm{C}^{\max} \end{aligned} \tag{2}$$

where C_i represents capacitor setting. Like T_i, C_i is non-continuous. $\mathrm{C}^{\max}$ is the maximum output of the bank capacitor.

2.3 Optimization using regulators, capacitors and PVs

This case considers tap changers, capacitors and reactive power output of the inverter-based PVs. The optimization model is given below.

$$\begin{aligned} \underset{X}{\text{minimize}} \ & \sum_{i=1}^{N} ||V_i - 1|| \\ \text{subject to} \ & 0.95 \leq V_i \leq 1.05 \\ & \mathrm{T}^{\min} \leq \mathrm{T}_i \leq \mathrm{T}^{\max} \\ & 0 < \mathrm{C}_i < \mathrm{C}^{\max} \\ & -{Q_{\mathrm{PV}}}^{\lim} \leq Q_{\mathrm{PV}} \leq {Q_{\mathrm{PV}}}^{\lim} \\ & {Q_{\mathrm{PV}}}^{\lim} = \mp\sqrt{({S_{\mathrm{PV}}}^{\max})^2 - (P_{\mathrm{PV}})^2} \end{aligned} \tag{3}$$

where P_{PV} and Q_{PV} represent the active and reactive power outputs of the PV, respectively, ${S_{\mathrm{PV}}}^{\max}$ represents the maximum apparent power of the PV and ${Q_{\mathrm{PV}}}^{\lim}$ shows the minimum and maximum limit values of the reactive power that PV can support.

3 GWO algorithm

The GWO [14] mimics the behavior of grey wolves. The algorithm relies on both their social hierarchy and the hunting process. Socially, grey wolves live as a group composed of 5–12 wolves. They have a social hierarchy between each other, and the highest ranked society members (leaders) are the alphas (α), who decide on hunting, sleeping location and so on. In the hierarchy, betas (β) are in the second level. They are candidates to become alphas when alphas die, or become very old. Betas help alphas in their decisions and give orders to lower-level wolves. The third level in the social hierarchy is the deltas (δ). They are sentinels, elders, caretakers and hunters. The lowest level in the social hierarchy is omegas (ω) [14]. The algorithm finds the best solutions and labels them α, β and ω appropriately at each iteration. Then the solution search process consists of encircling, hunting, attacking and searching.

The first step is the encircling of the prey. This is represented by equations [14]:

$$\vec{D} = |\vec{C}\,\vec{X}_p(t) - \vec{X}(t)| \tag{4}$$

$$\vec{X}(t+1) = \vec{X}_p(t) - \vec{A}\,\vec{D} \tag{5}$$

where t represents the current iteration, $\vec{A}$ $\vec{C}$ are coefficient vectors, $\vec{X}_p$ and $\vec{X}$ indicate the position vectors of the prey and the grey wolf, respectively, and D is the distance between the prey and the grey wolf. The coefficient vectors $\vec{A}$ and $\vec{C}$ can be calculated from [14]:

$$\vec{A} = 2\vec{a}\,\vec{r}_1 - \vec{a} \tag{6}$$

$$\vec{C} = 2\vec{r}_2 \tag{7}$$

where r_1 and r_2 are random vectors taking values between 0 and 1, and numerical values of $\vec{a}$ linearly decrease from 2 to 0 over the iterations.

The second step is hunting. In each iteration, the position of the prey is predicted by using the information of the distance of α, β, and δ to the prey. Then positions of the other elements are updated according to the 3 best positions. This is represented as follows [14]:

$$\begin{aligned} D_\alpha &= |C_1 X_\alpha - X|, \\ D_\beta &= |C_2 X_\beta - X|, \\ D_\delta &= |C_3 X_\delta - X| \end{aligned} \tag{8}$$

$$\begin{aligned} X_1 &= X_\alpha - A_1 D_\alpha, \\ X_2 &= X_\beta - A_2 D_\beta, \quad X_3 = X_\delta - A_3 D_\delta \end{aligned} \tag{9}$$

$$X_{t+1} = \frac{X_1 + X_2 + X_3}{3} \tag{10}$$

The next step is the attacking the prey, where $\vec{a}$ is reduced; hence, the range of $\vec{A}$ also decreases. When the range of $\vec{A}$ is between -1 and 1, the wolves are attacking. The search agent's next position will be between its current position and the prey's position. For global search purposes (exploration), the range of $\vec{A}$ is utilized with random values greater than 1 and less than -1.

The overall flowchart of algorithm is given in Fig. 1.

4 Application to voltage deviation minimization

4.1 Initialization

This step sets the population size, maximum number of iterations, initializes the parameters a, A, and C using Eqs. (6), (7), and initializes the wolf population elements for taps, capacitors and inverters depending on the problem. After initialization, a sample individual is:

$$\text{Individual}_i = [\mathrm{T}_1, \ldots, \mathrm{T}_n, \mathrm{C}_1, \ldots, \mathrm{C}_m, Q_{pv_1}, \ldots, Q_{pv_k}] \tag{11}$$

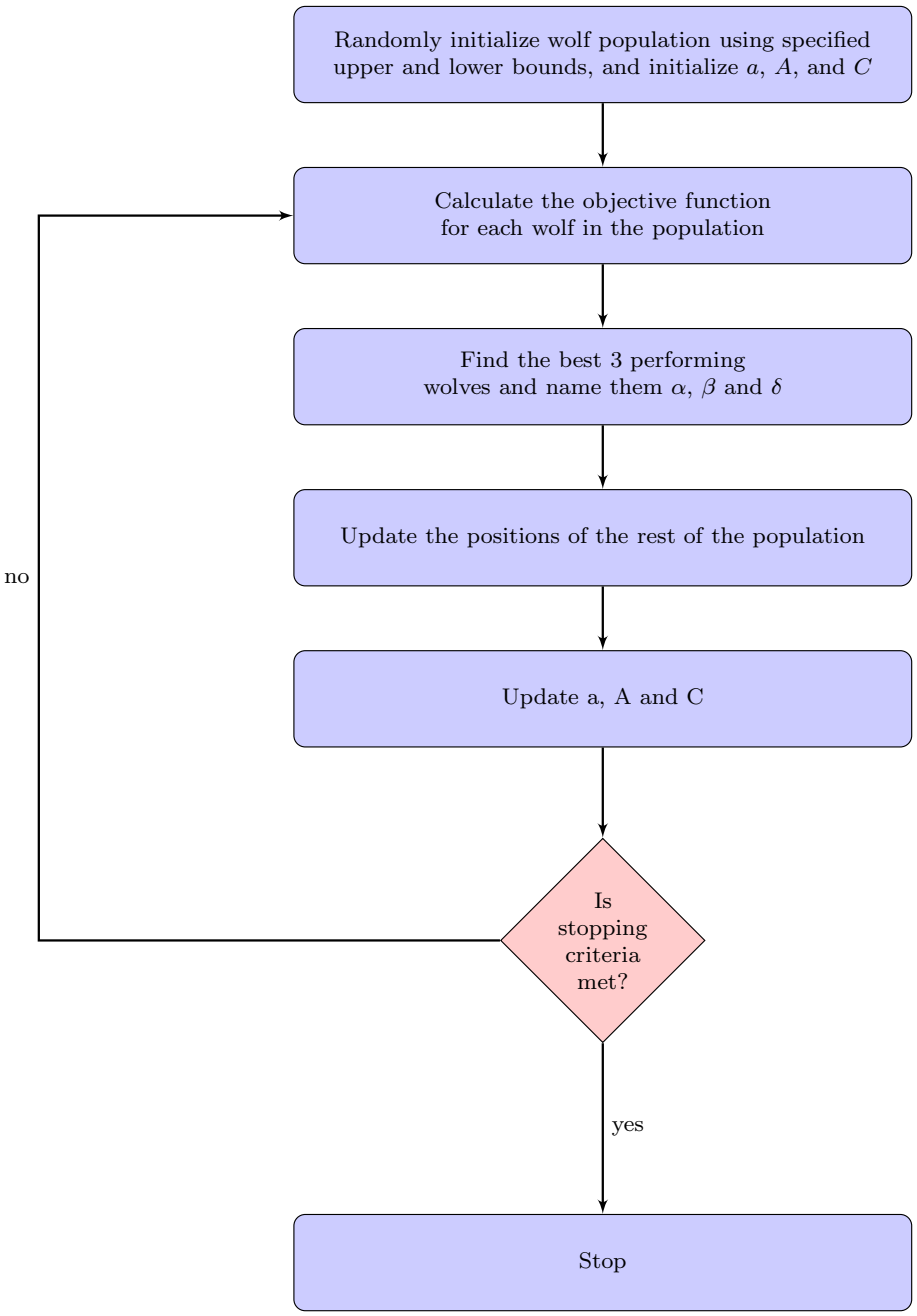

Fig. 1 Flowchart of GWO algorithm

where n, m, and k represent the number of voltage regulators, the number of bank capacitors, and the number of PVs in the system, respectively. Note that the initialization of tap positions is integer numbers limited between -16 and 16, capacitor positions integer numbers limited between 10 and 0. The limits of the reactive power outputs are determined by the inverter rating.

4.2 Calculation of objective function values

This step runs a load flow for each individual by using the design variables set in the previous step and computes the objective function of each individual. Note that the objective function is the sum of the absolute values of the deviation from desired voltage for all. From these objective function values, the best 3 solutions are selected. These individuals are specified as alpha α, beta β, and delta δ, respectively.

4.3 Position update by hunting

This step updates the positions using Eqs. (8)–(10). Then the values of the vectors a, A, and C are updated.

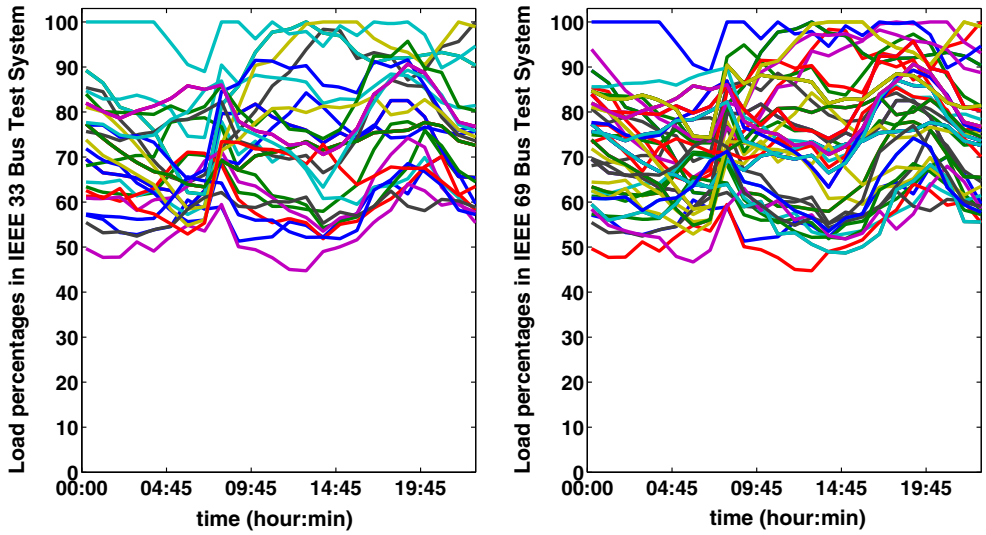

Fig. 2 Randomly obtained daily load profiles for buses in modified IEEE 33 and IEEE 69 bus test systems with 15 min intervals

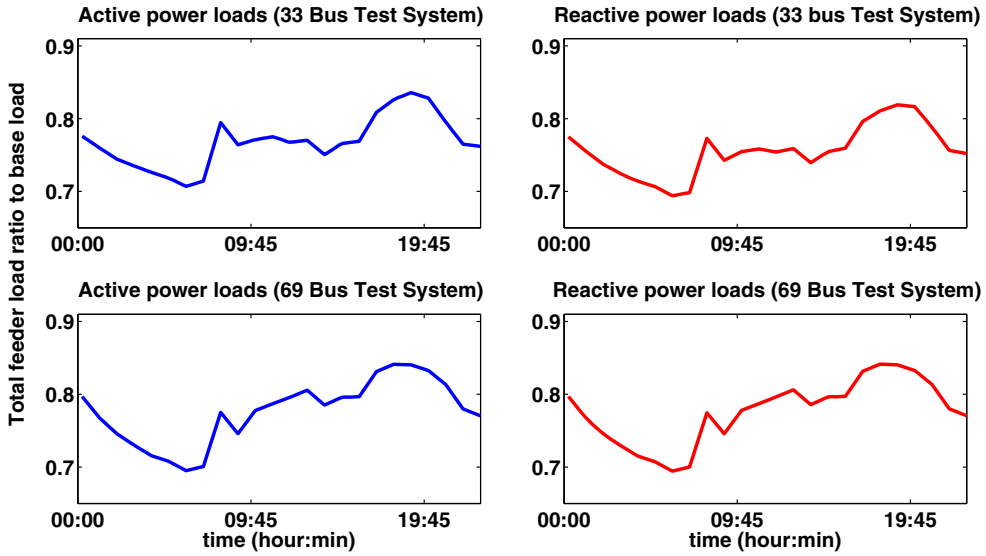

Fig. 3 Daily changes of total feeder loads compared to base case load profile

5 Test data

This study uses load data from [27] and PV power output data from NREL [28] to create a useful test dataset. The following describes the data manipulations to create the dataset.

5.1 Load data

Load profiles are created by applying the following procedure:

- Hourly data for one year are drawn from [27].
- Linear interpolation is used to create 15 min interval load data.
- Daily load data for each bus are selected randomly from yearly load data. In other words, n distinct integer random numbers are randomly selected from 1 to y, where n is the number of buses of the test system, and y is the number of days in a year.

Some example daily load profiles from [27] are shown in Fig. 2 for IEEE 33 and 69 bus test systems, where each individual line represents loads on individual buses.

We show active and reactive power load profiles of the both test feeders compared to the base cases for both systems in Fig. 3.

5.2 PV data

It is assumed that IEEE 33 bus system has 3 buses with PVs, and the IEEE 69 system has 6 buses with PVs. Each PV location has 10 PVs installed, each with a maximum capacity

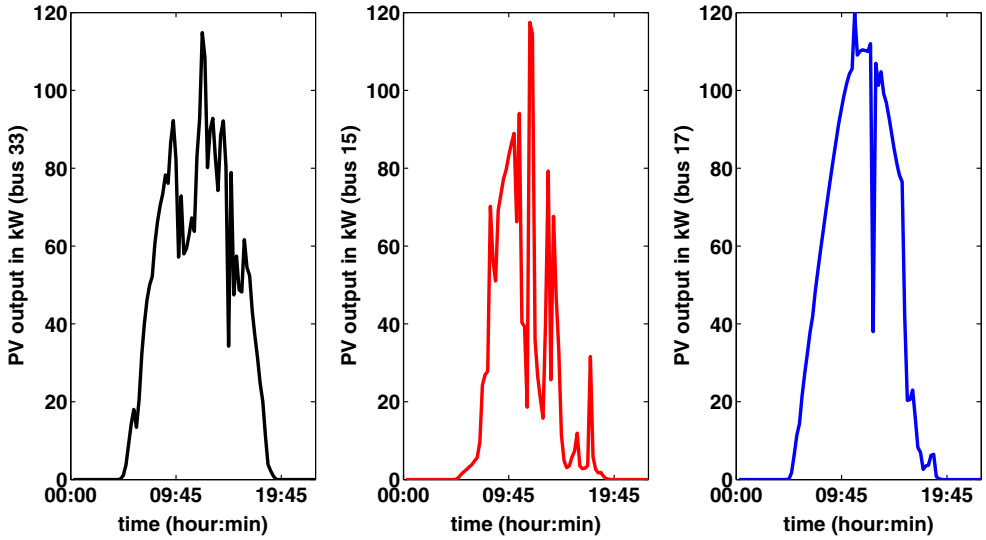

Fig. 4 Power outputs of PVs in modified IEEE 33 bus test system with 15 min intervals

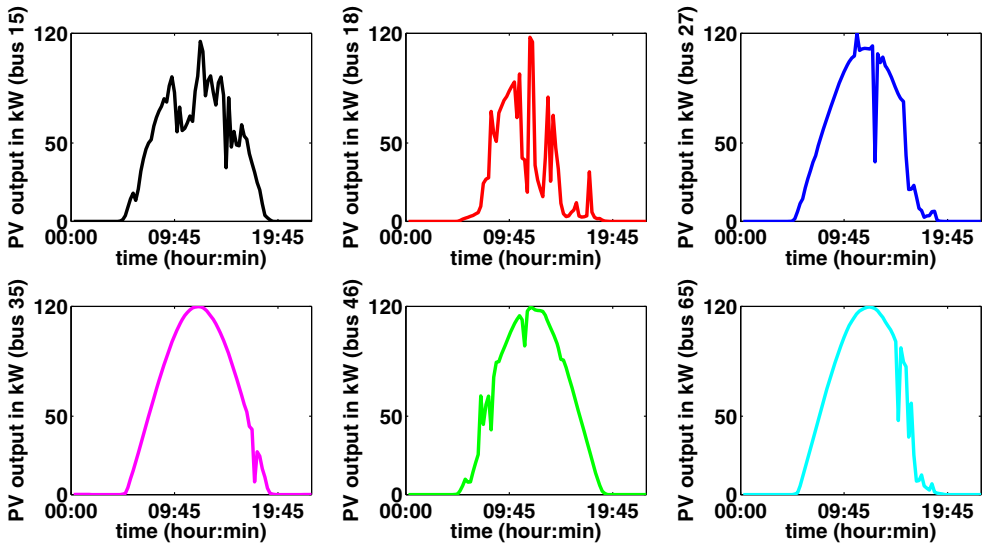

Fig. 5 Power outputs of PVs in modified IEEE 69 bus test system with 15 min intervals

of 120 kW. The simulation model assumes that daily PV outputs are forecasted. These power outputs are shown in Figs. 4 and 5. The output data were obtained randomly from several PV station irradiance output data in [28], and then these irradiance values were scaled as appropriate for the installed capacity.

6 Case studies

Proposed daily optimization model was tested on modified IEEE 33 [29] and IEEE 69 [30] bus test systems. We wrote a power flow code based on ladder iterative technique [31]. Details of the modifications on the systems, properties of the added tap changer transformers, bank capacitors and PVs are given together with the simulation results in the following subsections.

6.1 IEEE 33 bus test system simulations

The modified IEEE 33 Bus System is shown in Fig. 6. The total substation loads for the base configuration are 5084.26 kW and 2547.32 kVAR [29]. Two voltage regulators with tap changers between buses 5 and 6, and between buses 27 and 28 are added to the system. Two bank capacitors with maximum reactive power capability of 300 kVAR are added to buses 8 and 26. There are 3 PV stations each of them with 10 PVs with a maximum power of 120 kW located at buses 15, 17, and 33, respectively. Daily PV output data for these

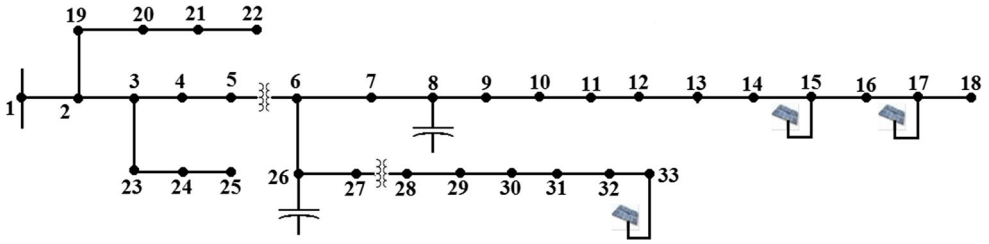

Fig. 6 Modified IEEE 33 bus test system

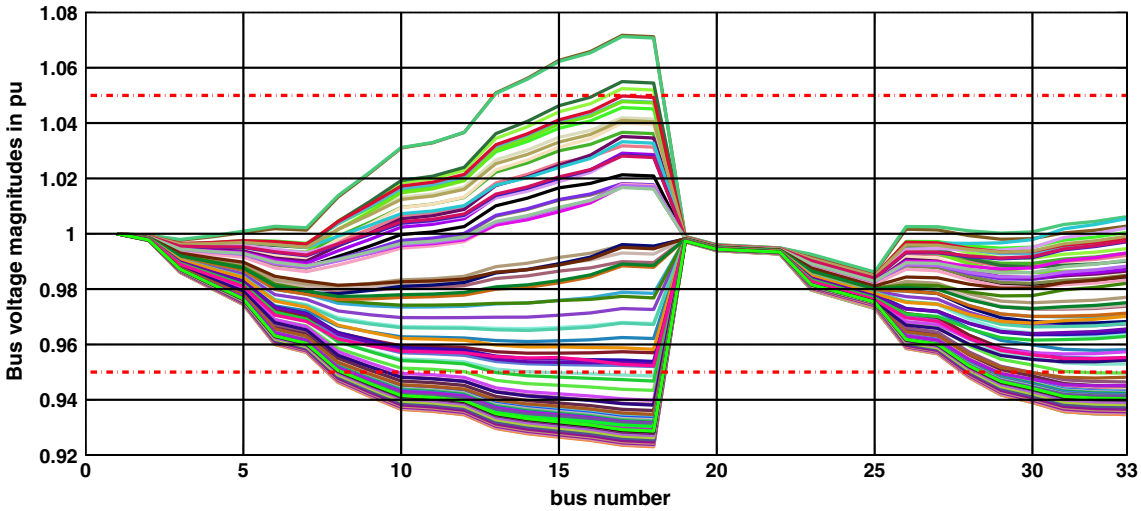

Fig. 7 Daily bus voltage magnitudes of IEEE 33 bus test system with no controls

buses were obtained from [32,33], and [34] for 20 May 2016, 20 May 2013 and 20 May 2011, respectively.

Initial simulations are performed to see the behavior of the system when there is no voltage control. For this aim, the tap and capacitor bank positions are set to zero, and it is assumed that PVs are not connected to the system. The simulation results are shown in Fig. 7. Note that each separate line in the figure represents the voltage magnitudes for each time interval. It is seen from the figure that there are both undervoltage and overvoltage problems at various times of the day.

Simulations are now performed considering various control devices. Note that taps of regulators are allowed to change in the range of −16 to 16, each with 0.015625 pu steps, and capacitors are allowed to change in the range of 0 to 10 each with 30 kVAR steps. The maximum power that a solar PV can generate is set to 120 kVA, and reactive power it can inject to the system is determined according to the power generated by the PV as follows: $Q_{\mathrm{PV}}{}^{\mathrm{lim}} = \mp\sqrt{(S_{\mathrm{PV}}{}^{\mathrm{max}})^2 - (P_{\mathrm{PV}})^2}$. Here, P_{PV} and Q_{PV} represent the active and reactive power outputs of the PV, respectively, $S_{\mathrm{PV}}{}^{max}$ represents the maximum apparent power of the PV and $Q_{\mathrm{PV}}{}^{\mathrm{lim}}$ shows the minimum and maximum limit values of the reactive power that PV can support.

The graphical representations of the voltage deviations in modified IEEE 33 bus system are shown in Fig. 8. The best voltage profile is obtained when tap changing regulators, capacitors, and reactive power outputs are all used for control. There is not much voltage improvement allowed by the shunt capacitors, since the installed capacitors are not close to PV panels.

The daily tap changes for the different cases are given in Fig. 9, where dashed and solid lines represent the tap changes for the tap changer transformers of branch 5–6 and branch 27–28, respectively. The number of tap changes for the first one is 32, 30 and 41 for Cases I, II and III, respectively. For the second transformer, these values are obtained as 35, 42, and 40 for Cases I, II and III, respectively. The number of tap operations do not change dramatically for these cases; however, the range of tap changing is reduced as more controllers are available.

Switched bank capacitor operations are given in Fig. 10, where dashed and solid lines represent the daily capacitor operations for switched capacitors installed on buses 8 and 26, respectively. The number of operations of capacitors is 45 and 19 for Case II. This number decreases to 14 and 10 when the inverters are controlled.

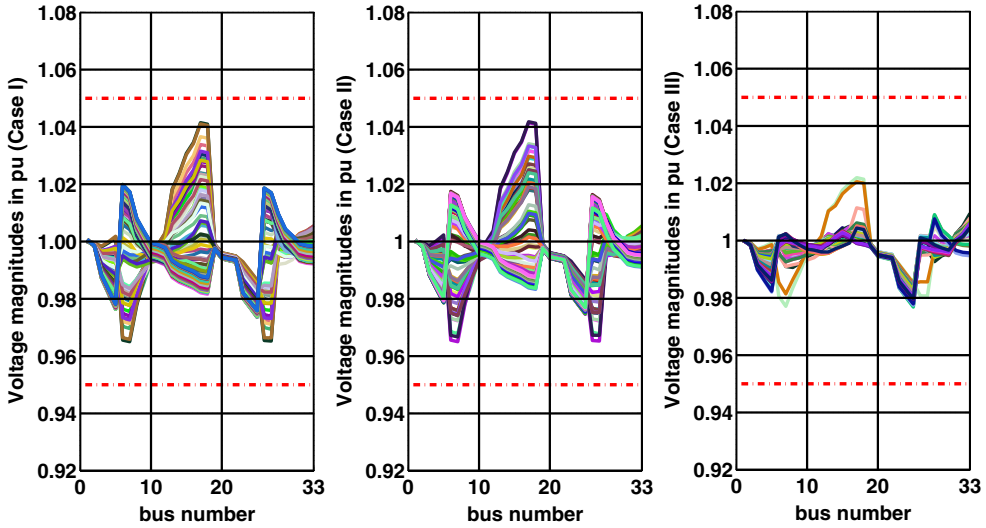

Fig. 8 Daily bus voltage magnitudes of IEEE 33 bus test system with different control devices

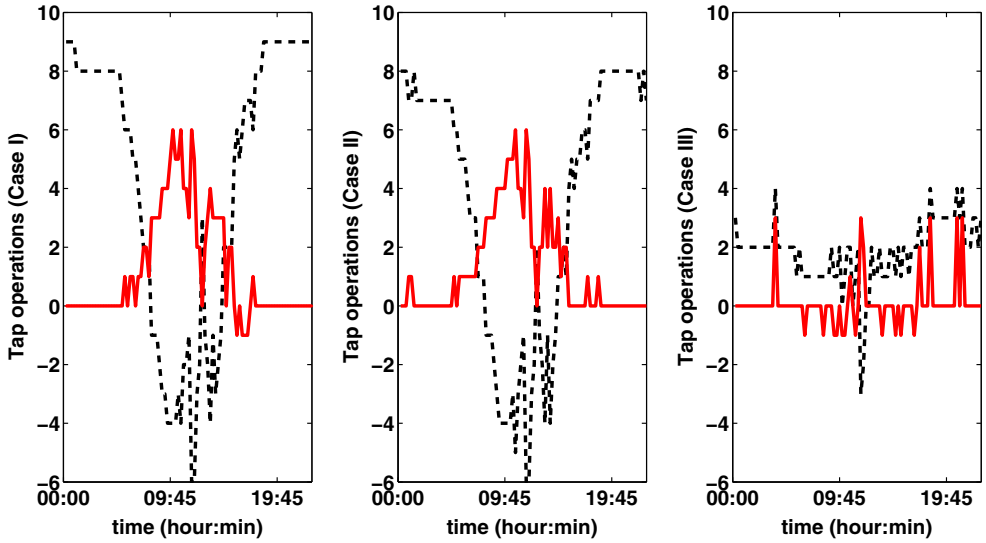

Fig. 9 Daily tap changes for 2 regulators

In Fig. 11, reactive power outputs of each PV on each PV installed bus in IEEE 33 bus system are illustrated. It can be seen that as the real power output from the PVs increases the reactive power support from the PVs decreases. Other PVs may start to absorb reactive power from the system when the PV active power outputs are close to maximum values.

6.2 IEEE 69 bus test system simulations

Figure 12 shows the modified IEEE 69 bus system. Detailed information on bus loads for this system is given above. Base case active load is 3802.19 kW, and reactive power load is 2694.60 kVAR [30]. The modified IEEE 69 Bus Test System includes three voltage regulators with tap changers between buses 5 and 6, between buses 13 and 14 and between buses 53 and 54. Four bank capacitors each with maximum reactive power capability of 300 kVAR and 10 tap changer positions are added to buses 20, 30, 40 and 60. The system includes 6 PV stations each of them with 10 PVs with a maximum power of 120 kW, on buses 15, 18, 27, 35, 46 and 65, respectively. Daily PV output data for these buses were obtained from [32–37] for 20 May 2016, 20 May 2013 and 20 May 2011, 20 May 2010, 20 May 2014 and 20 May 2012, respectively.

Similar to the tests performed for modified IEEE 33 Bus System, initial step for this case is running the daily load flow simulation when tap regulator and switched capacitor bank positions are set to zero, and PVs are not connected to the system. Simulation results that show bus voltage magnitudes with respect to 15 min time intervals are illustrated in Fig. 13. Note again, that each separate line in the figure represents the

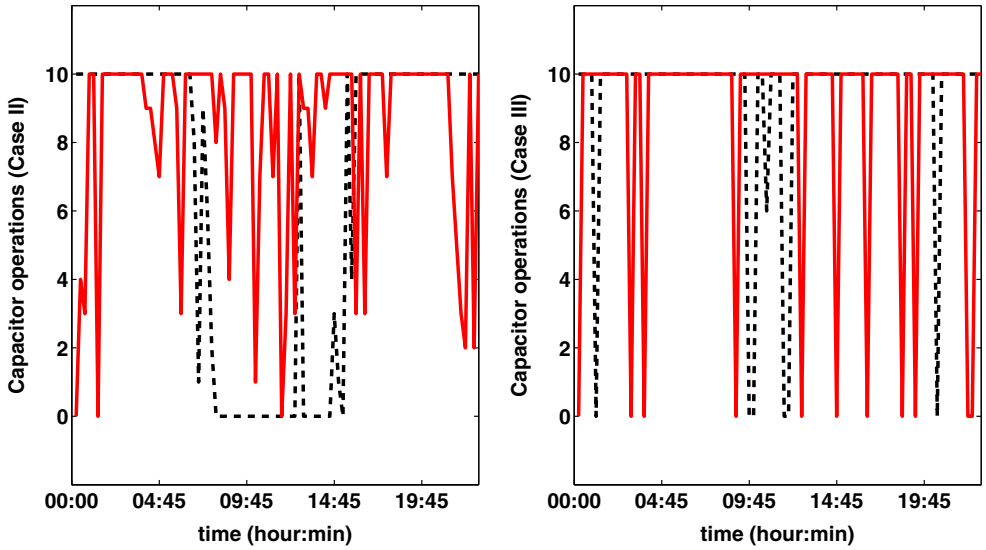

Fig. 10 Daily capacitor operations on IEEE 33 bus test system for 2 capacitors

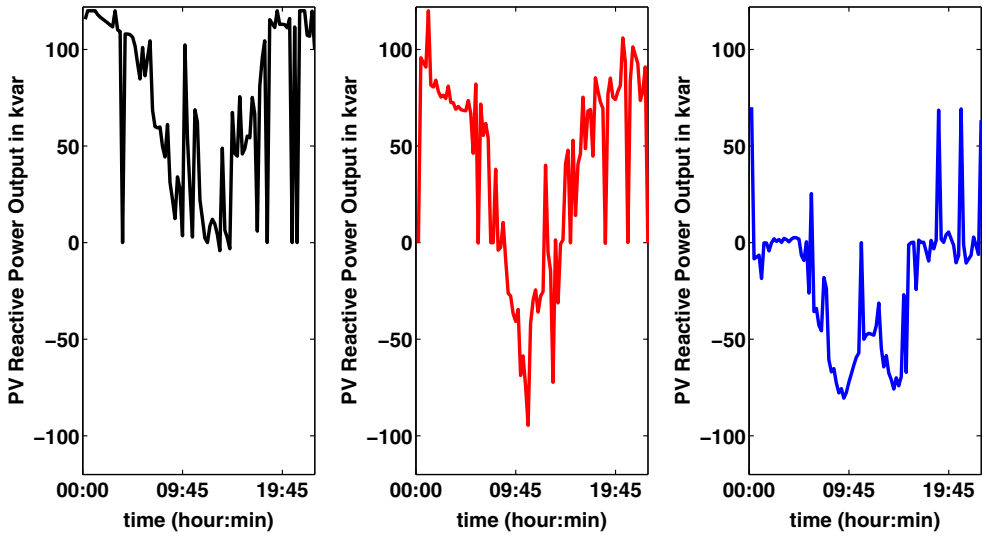

Fig. 11 Reactive power outputs of PVs on IEEE 33 bus test system

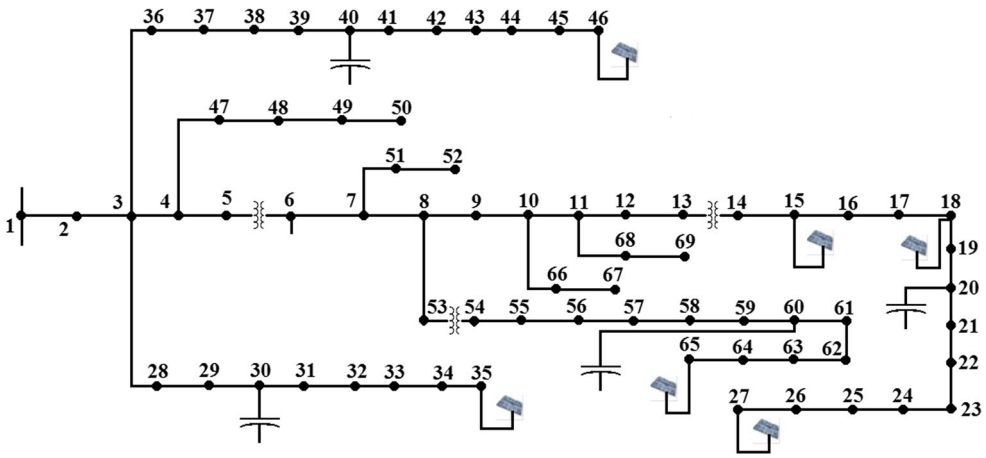

Fig. 12 Modified IEEE 69 bus test system

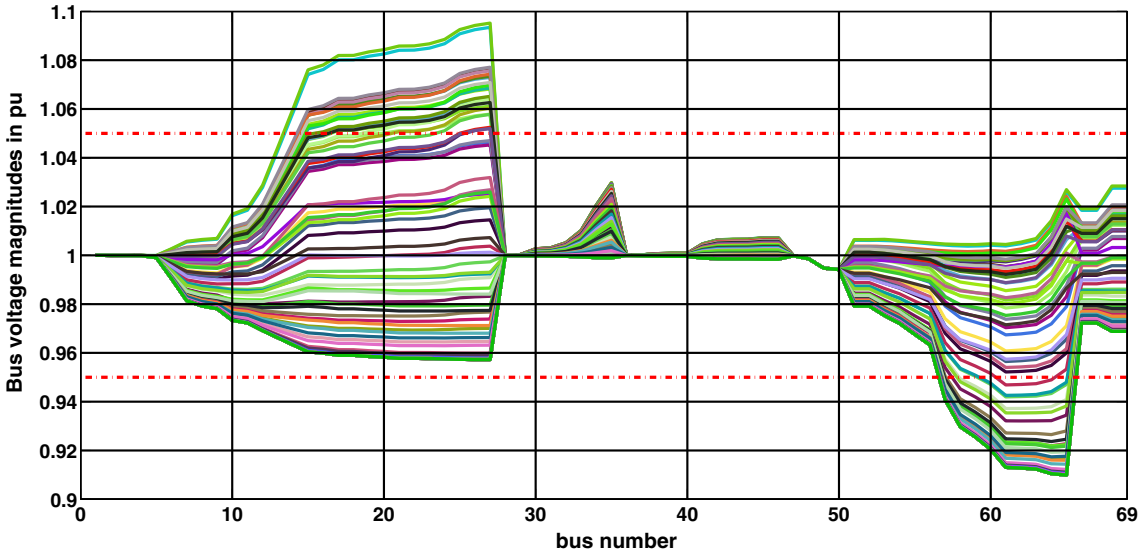

Fig. 13 Daily bus voltage magnitudes of IEEE 69 bus test system with no controls

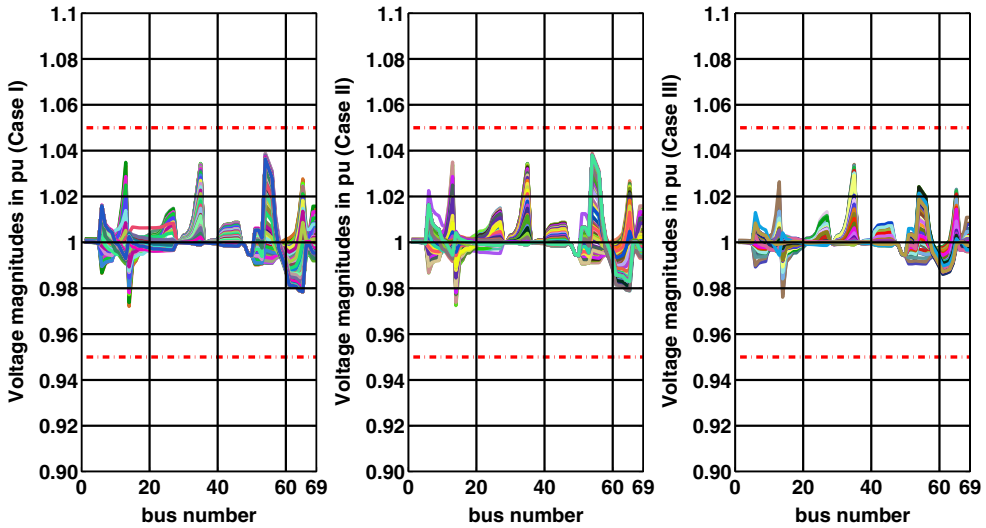

Fig. 14 Daily bus voltage magnitudes of IEEE 69 bus test system

voltage magnitudes for each time interval similar to 33 Bus Case. Voltage deviations in the figure show that this case has overvoltage and undervoltage profile problems. Hence, voltage profile must be adjusted by using taps, capacitors and/or PVs.

The simulation results for all cases are given in Fig. 14. The best voltage profile is obtained when all control types are used. It should be noted that even just using tap changes it is possible to bring the voltage profiles within the allowable range.

Daily tap changes of the regulators are shown in Fig. 15 for the different cases, where solid, dash-dotted and dashed lines represent the tap changes of the tap changer transformers of branch 5–6, 13–14, and 53–54, respectively. As expected, tap changer operations are performed over a wider range during the times that PVs produce more power and the load levels in the system are high.

There are four capacitors in the modified IEEE 69 bus system. Daily switched bank capacitor changes are shown in Fig. 16. Note that switched capacitor operations for the capacitors installed on buses 20 and 30 are represented in Figure. The number of capacitor switching operations actually increases when inverters are controlled as well. Our simulations with IEEE 69 Bus Test System use more PVs compared to IEEE 33 Bus Test System. As the fluctuations in loads and/or power outputs increase, the number of control actions taken also increase. Since the bank capacitors and voltage regulators are mechanical devices, it is not recommended to

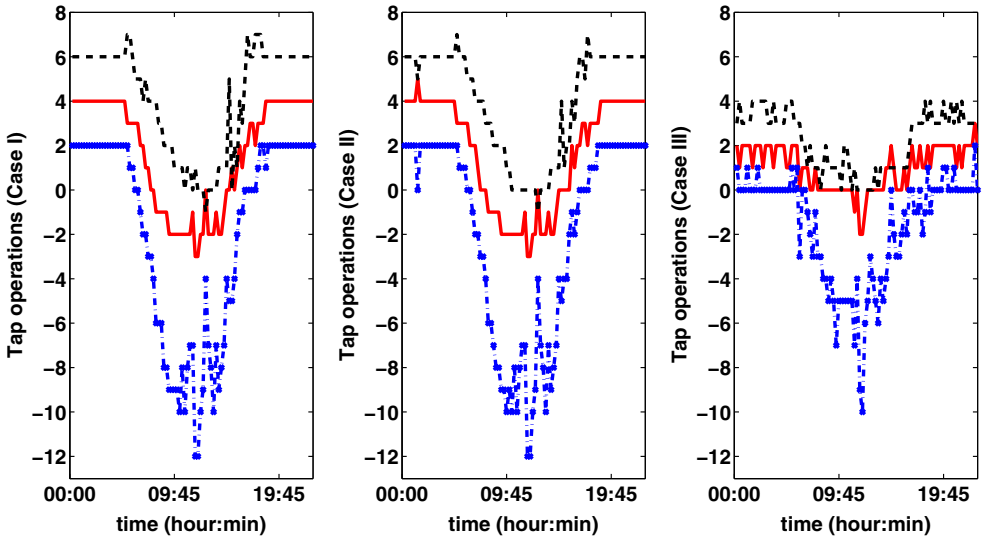

Fig. 15 Daily tap changes for 3 voltage regulators

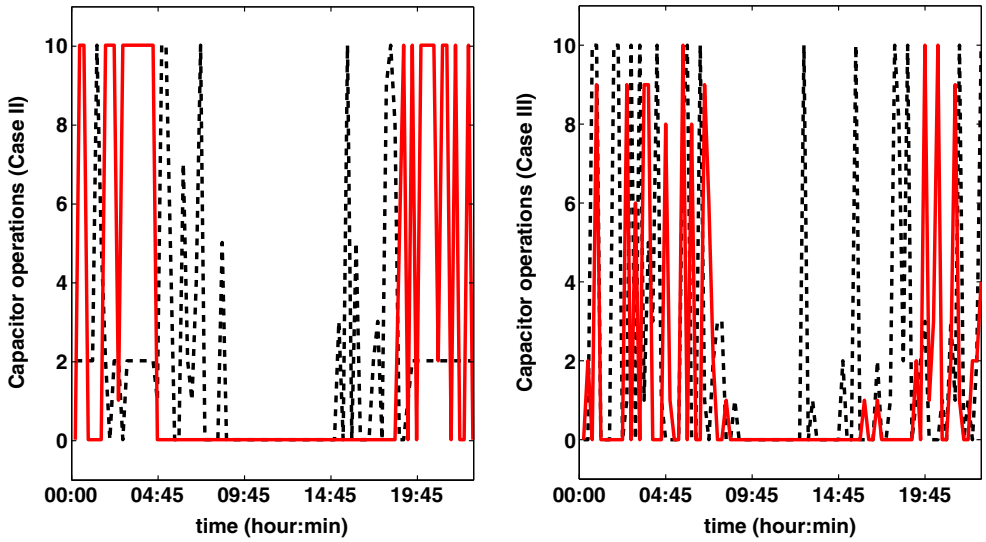

Fig. 16 Daily capacitor operations on IEEE 69 bus test system for 4 capacitors

frequently use them in modern distribution systems in order not to decrease their lifetimes.

Daily reactive power outputs of each of the PV in 6 buses are illustrated in Fig. 17. Here, similar to the previous case, reactive power support from the PVs decreases and starts to absorb reactive power as the PV active power outputs approaches their maximum value and the system load is close to its peak.

Solution quality and computational time efficiency of the simulation results by using GWO are compared to the differential evolution (DE) [11] and the harmony search (HS) [12] methods. The number of search agents and maximum number of iterations are selected as 30 and 1000 for GWO-based model both for simulations in IEEE 33 and 69 bus test systems. Harmony memory consideration rate (HMCR), pitch adjusting rate (PAR), harmony memory size (HMS) and maximum number of iterations are selected as 0.9, 0.30, 30, and 30000, respectively for the HS-based model in all simulations. Population size (Np), crossover rate (CR), scaling factor (F) and maximum number of iterations are selected as 30, 0.9 and 0.8, and 1000, respectively, for the DE-based model both for all simulations. Note that to be fair in the comparisons, the stopping conditions, populations sizes, maximum number of iterations are selected to be equal except since there is only one new function evaluation in HS the number of maximum iterations for this method is different than the other methods. Still the total number of function evaluations are enforced to be the same for all these 3 methods. The following tables and figures summarize these comparisons.

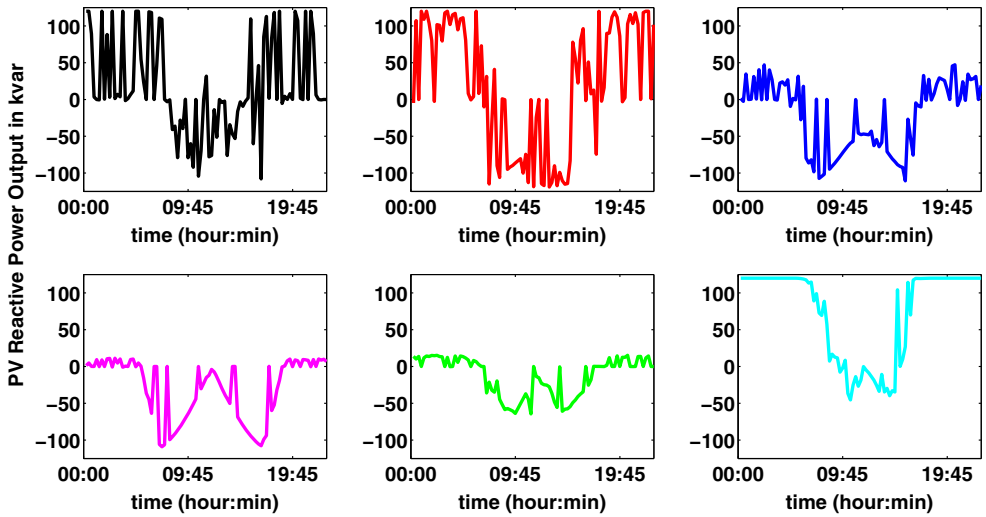

Fig. 17 Reactive power outputs of PVs on IEEE 69 bus test system

Table 1 Mean voltage magnitudes and standard deviations for IEEE 33 bus test system

	Case I	Std.	Case II	Std.	Case III	Std.
GWO	0.9960	0.0107	0.9964	0.0102	0.9969	0.0055
HS	0.9960	0.0107	0.9963	0.0099	0.9967	0.0061
DE	0.9960	0.0107	0.9964	0.0101	0.9968	0.0057

Table 2 Mean voltage magnitudes and standard deviations for IEEE 69 bus test system

	Case I	Std.	Case II	Std.	Case III	Std.
GWO	1.0002	0.0085	1.0009	0.0081	1.0001	0.0051
HS	1.0003	0.0085	1.0006	0.0081	1.0003	0.0059
DE	1.0004	0.0085	1.0009	0.0081	1.0001	0.0053

The mean voltage magnitudes and standard deviations of all simulations for the modified IEEE 33 bus test system is given in Table 1. Note that in both Tables 1 and 2 Std. represents standard deviation of the voltage magnitudes of the daily voltage magnitudes for Cases I, II and III. The GWO approach gives a slightly better numerical result in both average voltage profile and standard deviation, although all three methods give acceptable results.

Table 2 gives the numerical values that show the mean voltage magnitudes and standard deviations of all simulations for all case studies in the modified IEEE 69 bus test system. Again, the GWO solutions are slightly better since the standard deviation is somewhat lower.

Figure 18 shows the computational time on the modified IEEE 33 bus system. Each 15 min time interval simulation's computational time is found by dividing the total computational time by the number of time intervals in a simulated day. The DE-based model gives the worst computational time per 15 min interval. The computational times for GWO and HS are close to with GWO slightly faster for this test system.

Figure 19 illustrates the computational time results for the modified IEEE 69 bus distribution test system using the GWO, HS and DE models. Again, the DE approach gives the worst computational time. The computational times for GWO and HS are very close. HS is slightly better for this test system.

As stated in no free lunch theorem [38], one can not claim that there is a unique search algorithm that outperforms all the others for all cost functions. After the numerical tests for voltage deviation optimization problem in IEEE 33 and 69 test systems, we observed that GWO-based optimization approach solves the problem and might be an alternative to other methods.

7 Conclusion

This paper proposes a daily optimization model for power distribution systems using the GWO method. Different optimization models using tap changing regulators alone, tap changing regulators and switched capacitors together and tap changing regulators, switched capacitors and reactive power outputs of PV together are evaluated on modified IEEE 33 and IEEE 69 bus test systems. Detailed analysis from these simulations shows that the GWO adequately solves the optimization model. The best solution is obtained when tap changing regulators, switched capacitors and reactive power outputs of PVs are all taken into consideration. Comparing the GWO method with HS and DE in terms of numerical accuracy and simulation time, it is observed that the proposed GWO-based model gives accurate results and the simulation

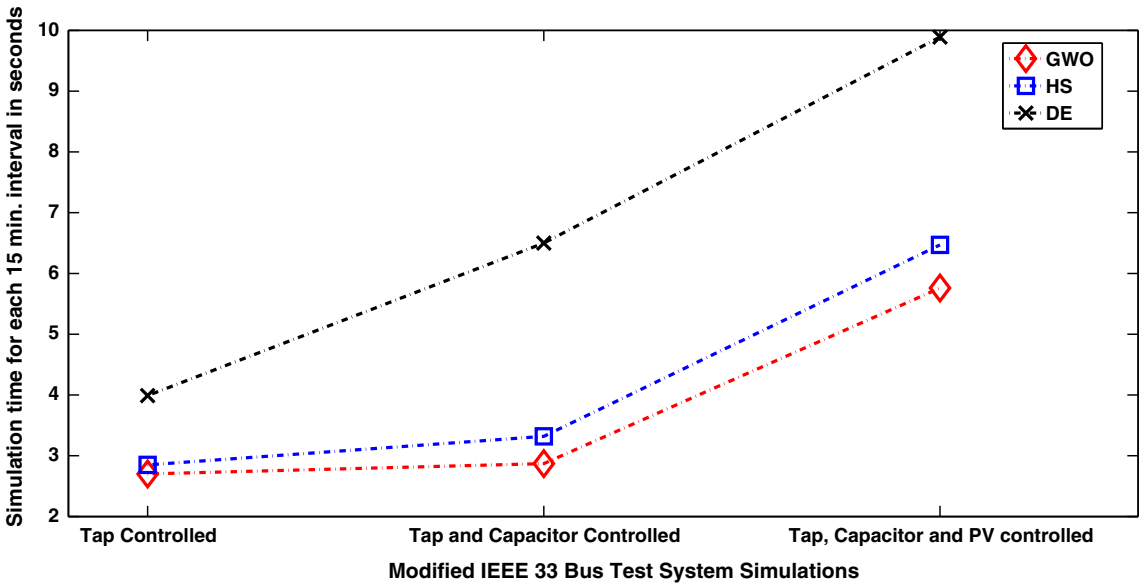

Fig. 18 Computational time results for three cases in IEEE 33 bus distribution systems

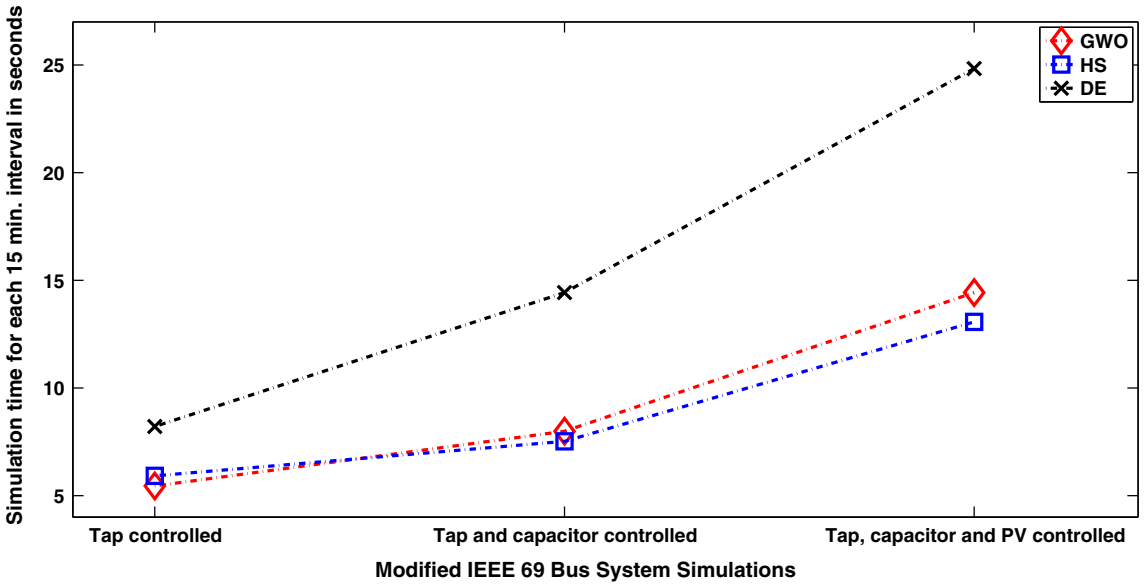

Fig. 19 Computational time results for three cases in IEEE 33 bus distribution systems

time of the model is faster than DE-based model and has minor differences with the HS-based model.

Acknowledgements This work was sponsored by the Office of Electricity Delivery & Energy Reliability, US Department of Energy under Contract No. DE-AC05-00OR 22725 with UT-Battelle and conducted at ORNL and UT Knoxville. This work also made use of Engineering Research Center Shared Facilities supported by the Engineering Research Center Program of the National Science Foundation and the Department of Energy under NSF Award Number EEC-1041877 and the CURENT Industry Partnership Program. The first author would like to thank the Scientific and Technological Research Council of Turkey (TUBITAK) for its financial support.

References

1. U.N.E. Programme, Global trends in renewable energy investment 2016, frankfurt school-unep centre bnef. Tech. rep. (2016). Accessed 10 Apr 2016
2. Katiraei F, Aguero JR (2011) Solar PV integration challenges. IEEE Power Energy Mag 9(3):62
3. Gonen T (2014) Electric power distribution engineering. CRC Press, Boca Raton
4. GmbH JSE (2016) Voltage regulated distribution transformer. Tech. rep. Accessed 10 Apr 2016
5. Mouli GRC, Bauer P, Wijekoon T, Panosyan A, Barthlein EM (2015) Design of a power-electronic-assisted OLTC for grid voltage regulation. IEEE Trans Power Deliv 30(3):1086

6. Rule 21 smart inverter working group technical reference materials, california energy commission. http://www.energy.ca.gov/electricity_analysis/rule21/ (2016). Accessed 12 Dec 2016
7. Ceylan O, Liu G, Xu Y, Tomsovic K (2014) Distribution system voltage regulation by distributed energy resources. In: 2014 North American power symposium (NAPS), Pullman, WA, pp 1–5. doi:10.1109/NAPS.2014.6965466
8. Liu G, Ceylan O, Xu Y, Tomsovic K (2015) Optimal voltage regulation for unbalanced distribution networks considering distributed energy resources. In: 2015 IEEE power & energy society general meeting, Denver, CO, pp 1–5. doi:10.1109/PESGM.2015.7286473
9. Rao SS (2009) Engineering optimization: theory and practice, 4th edn. Wiley, New York
10. Holland HJ (1992) Genetic algorithms. Sci Am 267:66–72
11. Storn R, Price K (1997) Differential evolution—a simple and efficient heuristic for global optimization over continuous spaces. J Glob Optim 11(4):341. doi:10.1023/A:1008202821328
12. Zong WG, Joong HK, Loganathan GV (2001) Simulation 76(2):60. http://sim.sagepub.com/content/76/2/60.abstract
13. Kennedy J, Eberhart R (1995) Particle swarm optimization. In: Proceedings of the IEEE international conference on neural networks, 1995, Perth, WA, vol 4, pp 1942–1948. doi:10.1109/ICNN.1995.488968
14. Mirjalili S, Mirjalili SM, Lewis A (2014) Grey wolf optimizer. Adv Eng Softw 69:46–61
15. Emary E, Zawbaa HM, Hassanien AE (2016) Binary grey wolf optimization approaches for feature selection. Neurocomputing 172:371
16. Rios LM, Sahinidis NV (2012) Derivative-free optimization: a review of algorithms and comparison of software implementations. J Glob Optim 56(3):1247. doi:10.1007/s10898-012-9951-y
17. Zhu Y, Tomsovic K (2007) Optimal distribution power flow for systems with distributed energy resources. Int J Electr Power Energy Syst 29(3):260
18. Ochoa LF, Dent CJ, Harrison GP (2010) Distribution network capacity assessment: variable DG and active networks. IEEE Trans Power Syst 25(1):87
19. Borghetti A, Bosetti M, Grillo S, Massucco S, Nucci CA, Paolone M, Silvestro F (2010) Short-term scheduling and control of active distribution systems with high penetration of renewable resources. IEEE Syst J 4(3):313
20. Calderaro V, Conio G, Galdi V, Massa G, Piccolo A (2014) Optimal decentralized voltage control for distribution systems with inverter-based distributed generators. IEEE Trans Power Syst 29(1):230
21. Agalgaonkar YP, Pal BC, Jabr RA (2014) Distribution voltage control considering the impact of PV generation on tap changers and autonomous regulators. IEEE Trans Power Syst 29(1):182
22. Kwang MAES, Lee Y (2008) Modern heuristic optimization techniques: theory and applications to power systems. Wiley, New York
23. Mohanty S, Subudhi B, Ray PK (2016) A new MPPT design using grey wolf optimization technique for photovoltaic system under partial shading conditions. IEEE Trans Sustain Energy 7(1):181
24. Sharma S, Bhattacharjee S, Bhattacharya A, Generation IET (2016) Grey wolf optimisation for optimal sizing of battery energy storage device to minimise operation cost of microgrid. Transm Distrib 10(3):625
25. Jayakumar N, Subramanian S, Ganesan S, Elanchezhian EB (2016) Grey wolf optimization for combined heat and power dispatch with cogeneration systems. Int J Electr Power Energy Syst 74:252
26. Sulaiman MH, Mustaffa Z, Mohamed MR, Aliman O (2015) Using the gray wolf optimizer for solving optimal reactive power dispatch problem Appl. Soft Comput 32:286
27. National grid load profiles. https://www9.nationalgridus.com/niagaramohawk/business/rates/5_load_profile.asp (2016). Accessed 03 Apr 2016
28. Nrel, measurement and data center. http://www.nrel.gov/midc/ (2016). Accessed 10 June 2016
29. Baran ME, Wu FF (1989) Network reconfiguration in distribution systems for loss reduction and load balancing. IEEE Trans Power Deliv 4(2):1401. doi:10.1109/61.25627
30. Baran ME, Wu FF (1989) Optimal capacitor placement on radial distribution systems. IEEE Trans Power Deliv 4(1):725. doi:10.1109/61.19265
31. Kersting WH (2012) Distribution system modeling and analysis. CRC Press, Boca Raton
32. Andreas A, Wilcox S (2016) Solar technology acceleration center (solartac), aurora, colorado (data). Tech. Rep. DA-5500-56491, NREL. doi:10.5439/1052224
33. Lowry range solar station, colorado state land board. doi:10.5439/1052550 (2014). Accessed 11 June 2016
34. Xcel energy comanche station. http://www.nrel.gov/midc/xecs (2011). Accessed 11 June 2016
35. Sun spot one san luis valley, colorado. http://www.nrel.gov/midc/ss1 (2010). Accessed 11 June 2016
36. Andreas A, Wilcox S (2016) Solar resource and meteorological assesment project (solrmap), rotating shadowband radiometer (rsr), los angeles, california (data). Tech. Rep. DA-5500-56502, NREL. doi:10.5439/1052230
37. Solar resource and meteorological assesment project, tri-state, ecalante. doi:10.5439/1052229 (2013). Accessed 11 June 2016
38. Wolpert DH, Macready WG (1995) No free lunch theorems for search. Technical Report SFI-TR-95-02-010, Santa Fe Institute, 1995. https://pdfs.semanticscholar.org/bfd2/88d7adb887ea0c91d14131f4cb78d675f0a4.pdf